One Body Density Matrix, Natural Orbits and Quasi Hole States in ^{16}O and ^{40}Ca

A. Fabrocini[1)] and G.Co'[2)]

[1)] *Dipartimento di Fisica, Università di Pisa,*
and Istituto Nazionale di Fisica Nucleare, sezione di Pisa,
I-56100 Pisa, Italy

[2)] *Dipartimento di Fisica, Università di Lecce*
and Istituto Nazionale di Fisica Nucleare, sezione di Lecce,
I-73100 Lecce, Italy

The one body density matrix, momentum distribution, natural orbits and quasi hole states of ^{16}O and ^{40}Ca are analyzed in the framework of the correlated basis function theory using state dependent correlations with central and tensor components. Fermi hypernetted chain integral equations and single operator chain approximation are employed to sum cluster diagrams at all orders. The optimal trial wave function is determined by means of the variational principle and the realistic Argonne v_8' two–nucleon and Urbana IX three–nucleon interactions. The correlated ^{16}O momentum distribution is in good agreement with the variational Monte Carlo results and shows the well known enhancement at large momentum values with respect to the independent particle model. A similar behavior is found in ^{40}Ca. The relative importance of the different types of correlations (mainly Jastrow and tensor) on the momentum distribution appears to be similar in the nuclei and in nuclear matter. Diagonalization of the density matrix provides the natural orbits and their occupation numbers. Correlations deplete the occupation number of the first natural orbitals by more than 10%. The first following ones result instead occupied by a few percent. The single particle overlap functions and the spectroscopic factors are computed in the correlated model for both nuclei and compared with previous estimates. Jastrow correlations lower the spectroscopic factors of the valence states by a few percent ($\sim 1-3\%$) with respect to unity. An additional $\sim 8-12\%$ depletion is provided by spin–isospin tensor correlations. It is confirmed that a variational teatment of short range correlations does not explain the spectroscopic factors extracted from $(e,e'p)$ experiments. Such an approach corresponds to the zeroth order of the correlated basis function theory and two–hole one–particle perturbative corrections in the correlated basis are expected to provide most of the remaining strength, as in nuclear matter.

I. INTRODUCTION

The notion of nuclei as a set of mutually, strongly interacting particles is now generally accepted and it is widely recognized that correlations beyond the mean field play a substantial, if not decisive, role in the microscopic description of nuclear properties. This is intuitive when energies are evaluated, but there are also clear signatures of the presence of correlations in some quantities related to the behavior of the single nucleon in the medium. For instance, it is known that the one nucleon momentum distribution (MD) has dominant high momentum components which are due to short range nucleon–nucleon (NN) correlations and are not describable in any independent particle model (IPM) [1,2]. In addition, NN correlations may be responsible for the reduction of the spectroscopic strengths of the hole states [3].

The ideal way of describing the nucleus would consist in solving the many–body Schrödinger equation with realistic interactions. Exact solutions have been obtained in light nuclei up to A=8 within a variety of methods: quantum Monte Carlo [4,5], Faddeev–like [6] and correlated hyperspherical harmonics [7] expansions.

The treatment of heavier nuclei has not yet attained the same degree of accuracy as the light ones. However, the situation is rapidly improving, at least for doubly closed shell nuclei. The ^{16}O nucleus has been studied by variational Monte Carlo [8] (VMC) and coupled cluster [9] methods. The variational theory underlying the correlated basis function (CBF) [10] method has been used in doubly closed shell nuclei by Fermi hypernetted chain (FHNC) integral equations [11,12]. The same accuracy as in the best variational studies of nuclear matter has been obtained in ^{16}O and ^{40}Ca by using spin and isospin dependent correlations and modern, microscopic potentials [13]. To this aim, the nuclear matter single operator chain approximation [14] has been extended to finite nuclear systems to deal with state dependent correlations in the framework of the FHNC technique [15] (FHNC/SOC). The variational and the coupled cluster approaches have provided an overall satisfying description of such ground state properties as binding energies, one– and two–body densities and structure functions.

In medium heavy nuclei the microscopic approach has to be compared with the independent particle model and its description of various nuclear features. The use of this model is so wide and well–established that great part of the nomenclature on medium and heavy nuclei is based upon concepts defined within the IPM itself. For example, the ideas of collective excitations, single particle levels, occupation probabilities and spectroscopic factors are meaningful only in a theoretical framework where the IPM is a first order approximation.

The sources of effects beyond the IPM description are generally termed as correlations. This name is hiding two rather different kinds of physical effects. Long range correlations are generated by the so–called residual interaction, neglected in the IPM and reponsible for the collective excitations. The short range correlations (SRC) are mainly produced by the repulsive core of the nucleon–nucleon interaction. Moreover, important non central components at intermediate range are needed for most realistic descriptions. While collective phenomena have been known since the early times of nuclear physics, effects produced by the SRC are more difficult to be experimentally singled out. Only in these last few years, thanks to the advances of the experimental techniques, there have been some consistent effort aimed to their identification.

The sensitivity of the two–nucleon emission cross section to the SRC is evident [16], but also other quantities related to the behavior of the single nucleon in the medium seem to depend on them. For instance, $(e, e'p)$ data in the quasi-elastic region need a consistent reduction of the IPM hole strength to be reproduced [17]. The same holds for the electromagnetic form factors of low lying states with high angular momentum [18]. Furthermore, charge density distributions obtained by elastic electron scattering experiments are, in the nuclear interior, smaller than those predicted by the IPM [19]. All these facts could be explained by assuming occupation probabilities of the single particle levels different from that of the IPM [20].

From the theoretical point of view, the basic quantity to be investigated in order to verify the hypothesis of partial occupation probability is the one body density matrix (OBDM), $\rho(\mathbf{r}_1, \mathbf{r}_{1'})$. defined as:

$$\rho(\mathbf{r}_1, \mathbf{r}_{1'}) = \langle \Psi_0(A) | a^\dagger(\mathbf{r}_1) a(\mathbf{r}_{1'}) | \Psi_0(A) \rangle \,, \tag{1}$$

where $\Psi_0(A)$ is the ground state A–body wave function and $a^\dagger(\mathbf{r}_1)$ is the creation operator of a nucleon at the position $\mathbf{r}_1$. Much theoretical effort has been devoted to understand the behavior of the OBDM and of the momentum distribution (MD), $n(k)$, given by the Fourier transform of $\rho(\mathbf{r}_1, \mathbf{r}_{1'})$. The MD is also obtained by the energy integral of the spectral function, that is often used in plane wave impulse approximation to study inclusive and exclusive reactions. In some approximations and kinematics, the MD is directly employed. The natural orbits (NO) [21], with their occupation numbers (n_α), are defined as the basis where the OBDM is diagonal. In the IPM, the nuclear ground state is described by a Slater determinant of fully occupied single particle (SP) wave functions below the Fermi surface, α_F. In this case, the NO and the SP w.f. coincide and $n_{\alpha \leq \alpha_F}$=1 and $n_{\alpha > \alpha_F}$=0. Deviations from this situation are a measure of the correlations, since they allow higher NO to become populated with $n_\alpha \neq$0.

Quantities not directly related to the OBDM, but accessible to the experimental investigation by means of knock out experiments, are the quasihole (QH) wave functions, $\psi_h(\mathbf{r})$, defined as the overlaps between Ψ_0 and the hole states, Ψ_h, produced by removing a nucleon from the position $\mathbf{r}$. From $(e, e'p)$ experiments it is possible to obtain an accurate determination of the QH overlap functions [22]. Their normalizations give the spectroscopic factors, S_h, that deviate from unity (the IPM value) because of various effects, from center of mass to correlation corrections. Typical values extracted from the experiments are $S_h \sim 0.6 - 0.7$ [23], and their correct calculation represents a severe challenge for the available many–body theories.

The FHNC theory for the OBDM in correlated infinite matter was developed by Fantoni [24]. Subsequently, FHNC/SOC was applied to nuclear matter to calculate both the MD [25] and the spectral function [26]. The technique has been then extended to evaluate the OBDM in doubly closed shell nuclei described by a correlated wave function containing scalar, spin–isospin independent (or Jastrow) correlations [27]. Isospin dependence was later introduced to treat closed shell nuclei in the jj coupling scheme [12]. The ^{16}O momentum distribution has been calculated by using state dependent correlations [8] within the VMC approach. Low order cluster expansions have been employed in closed shell nuclei [51,29] and in sp and sd shell nuclei with N=Z [30]. Local density approximation was used to estimate the MD in medium–heavy nuclei [31] from the nuclear matter results. The effect of short range correlations on the OBDM and the NO in ^{16}O has been studied by means of the Green function method [32]. As far as the overlap functions are concerned, in the ^{7}Li$(e, e'p)^6$He reaction the experimental data have been succesfully compared with the VMC, parameter–free theoretical predictions [33]. VMC has been used also in the analysis of the ^{16}O$(e, e'p)$ knockout experiments [34]. A relationship between the OBDM and the QH overlaps [35] has been recently exploited [36,37] to evaluate the spectroscopic factors for the same reaction, using several correlated models for the density matrix. The effect of long–range correlations has been considered in Refs. [38,36].

In this paper we extend the FHNC/SOC methodology to deal with the OBDM of ^{16}O and ^{40}Ca using wave functions with central and tensor correlations. The correlated A–body wave function, $\Psi_0(1,2...A)$, is written as:

$$\Psi_0(1,2...A) = G(1,2...A)\Phi_0(1,2...A)\,, \tag{2}$$

where $G(1,2...A)$ is a many–body correlation operator acting on the mean field wave function $\Phi_0(1,2...A)$, given by a Slater determinant of single particle wave functions, $\phi_\alpha(i)$. The correlation operator is given by a symmetrized product of two-body correlation operators, F_{ij},

$$G(1,2...A) = \mathcal{S}\left[\prod_{i<j} F_{ij}\right]. \tag{3}$$

In the most sophisticated variational calculations (both in nuclear matter and in nuclei) F_{ij} assumes the form:

$$F_{ij} = \sum_{p=1,8} f^p(r_{ij}) O^p_{ij}\,. \tag{4}$$

where

$$O^{p=1,8}_{ij} = [1, \boldsymbol{\sigma}_i\cdot\boldsymbol{\sigma}_j, S_{ij}, (\mathbf{L}\cdot\mathbf{S})_{ij}] \otimes [1, \boldsymbol{\tau}_i\cdot\boldsymbol{\tau}_j] \tag{5}$$

and $S_{ij} = (3\,\hat{\mathbf{r}}_{ij}\cdot\boldsymbol{\sigma}_i\,\hat{\mathbf{r}}_{ij}\cdot\boldsymbol{\sigma}_j - \boldsymbol{\sigma}_i\cdot\boldsymbol{\sigma}_j)$ is the tensor operator. The spin–orbit components will be omitted in this paper (f_6 model).

The variational principle allows for fixing the correlation functions, $f^p(r)$, and the single particle wave functions by minimizing the ground state energy,

$$E[\Psi_0] = \frac{\langle\Psi_0|H|\Psi_0\rangle}{\langle\Psi_0|\Psi_0\rangle}\,. \tag{6}$$

In our calculation we adopt a non relativistic nuclear hamiltonian of the form:

$$H = \frac{-\hbar^2}{2\,m}\sum_i \nabla_i^2 + \sum_{i<j} v_{ij} + \sum_{i<j<k} v_{ijk}\,. \tag{7}$$

Modern two–nucleon potentials, v_{ij}, are built on the very high quality phase–shift analyses of the NN scattering data [39,40]. We have used the v_8' reduction of the Argonne v_{18} [41] potential. For the three–nucleon interaction the Urbana IX model [5] has been adopted.

The plan of the paper is as follows: section 2 is devoted to a brief description of the FHNC/SOC theory for the OBDM; in section 3 the results obtained for the ^{16}O and ^{40}Ca momentum distributions and natural orbits are presented and discussed; in section 4 we describe the FHNC theory for the overlap functions and give the results for the spectroscopic factors; the conclusions are drawn in section 5.

II. FHNC/SOC THEORY FOR THE ONE BODY DENSITY MATRIX

The one body density matrix (1) may be written as

$$\rho(\mathbf{r}_1,\mathbf{r}_{1'}) = \frac{A}{\mathcal{N}}\int d^3r_2...\int d^3r_A\,\Psi_0^\dagger(1,2,..A)\Psi_0(1',2,..A)\,, \tag{8}$$

where $\mathcal{N} = \int d^3r_1...\int d^3r_A|\Psi_0|^2$. The one body density, $\rho_1(\mathbf{r}_1)$, is the diagonal part of the OBDM, whose Fourier transform gives the momentum distribution,

$$n(k) = \frac{1}{A}\int d^3r_1\int d^3r_{1'}\,\rho(\mathbf{r}_1,\mathbf{r}_{1'})\,e^{i\mathbf{k}\cdot(\mathbf{r}_1-\mathbf{r}_{1'})}\,. \tag{9}$$

In the independent particle model, the OBDM is given by:

$$\rho_{IPM}(\mathbf{r}_1,\mathbf{r}_{1'}) = \sum_\alpha \phi^\dagger_\alpha(1)\phi_\alpha(1') = \Big(\sum_{\sigma\tau} \chi^\dagger_{\sigma\tau}(1)\chi_{\sigma\tau}(1')\Big) N_0(\mathbf{r}_1,\mathbf{r}_{1'})\,, \tag{10}$$

and

$$\rho_{1,IPM}(\mathbf{r}_1) = \sum_\alpha |\phi_\alpha(1)|^2 = \nu N_0(\mathbf{r}_1,\mathbf{r}_1)\,, \tag{11}$$

where $\chi_{\sigma\tau}(1)$ is the spin–isospin single particle eigenfunction and ν the degeneracy number ($\nu = 4$, for the doubly closed shell, N=Z nuclei we are considering). The second equalities in the above equations are valid since we are working in ls coupling.

In analogy, we define the function $N(\mathbf{r}_1,\mathbf{r}_{1'})$ via the relation:

$$\rho(\mathbf{r}_1,\mathbf{r}_{1'}) = \Big(\sum_{\sigma\tau} \chi^\dagger_{\sigma\tau}(1)\chi_{\sigma\tau}(1')\Big) N(\mathbf{r}_1,\mathbf{r}_{1'})\,. \tag{12}$$

We have already presented in Ref. [27] the FHNC theory of the OBDM for Jastrow correlated wave functions,

$$G_J(1,2...A) = \prod_{i<j} f^1(r_{ij})\,, \tag{13}$$

having only the $p = 1$ scalar component in the correlation factor F_{ij}. The density matrix is expanded in powers of the *dynamical correlations*, $h(r) = [f^1(r)]^2 - 1$ (h–bond) and $\omega(r) = f^1(r) - 1$ (ω–bond), and of the *statistical correlations*, $N_0(\mathbf{r}_i,\mathbf{r}_j)$ (exchange or e–bonds). The expansion generates cluster terms classified according to the number of particles and to the number of the correlations. The FHNC equations allow for summing cluster terms at all orders. Details of the finite systems FHNC theory may be found in [27] and in Ref. [11].

The FHNC/SOC equations for the more general f_6 correlation were derived in Ref. [15] for the one and two body densities. In the case of the OBDM, we can write

$$\begin{aligned} N(\mathbf{r}_1,\mathbf{r}_{1'}) &= \xi^c_\omega(\mathbf{r}_1)[1+\Delta\xi^{op}_\omega(\mathbf{r}_1)]\xi^c_\omega(\mathbf{r}_{1'})[1+\Delta\xi^{op}_\omega(\mathbf{r}_{1'})]e^{N^c_{\omega\omega}(\mathbf{r}_1,\mathbf{r}_{1'})} \\ &\times \Big[N_0(\mathbf{r}_1,\mathbf{r}_{1'}) - N^c_{\omega_c\omega_c}(\mathbf{r}_1,\mathbf{r}_{1'})\Big] + \xi^c_\omega(\mathbf{r}_1)\xi^c_\omega(\mathbf{r}_{1'})e^{N^c_{\omega\omega}(\mathbf{r}_1,\mathbf{r}_{1'})} \\ &\times \sum_{p\ge 2} A^p\Delta^p\Big\{N^p_{\omega\omega}(\mathbf{r}_1,\mathbf{r}_{1'})\Big[N_0(\mathbf{r}_1,\mathbf{r}_{1'}) - N^c_{\omega_c\omega_c}(\mathbf{r}_1,\mathbf{r}_{1'})\Big] - N^p_{\omega_c\omega_c}(\mathbf{r}_1,\mathbf{r}_{1'})\Big\}\,. \end{aligned} \tag{14}$$

$N^p_{\omega\omega}$ and $N^p_{\omega_c\omega_c}$ are *nodal* functions (see [27]) of the $\omega\omega$ and $\omega_c\omega_c$ type, ξ^c_ω and $\Delta\xi^{op}_\omega$ are the central vertex corrections and their operatorial contributions [25] and the matrices A^p and Δ^p are defined in [15]. The components will be often labelled as c ($p = 1$) and σ (spin), τ (isospin) and t (tensor).

The nodal funtions are obtained by the equations:

$$N^p_{\omega\omega}(\mathbf{r}_1,\mathbf{r}_{1'}) = \sum_{xx'}\sum_{qr}\int d^3r_2\xi^{qrp}_{121'}X^q_{\omega x}(\mathbf{r}_1,\mathbf{r}_2)V^{qr}_{xx'}(\mathbf{r}_2)\left[X^r_{x'\omega}(\mathbf{r}_2,\mathbf{r}_{1'}) + N^r_{x'\omega}(\mathbf{r}_2,\mathbf{r}_{1'})\right]\,, \tag{15}$$

and

$$\begin{aligned} N^p_{\omega_c\omega_c}(\mathbf{r}_1,\mathbf{r}_{1'}) &= \sum_{qr}\int d^3r_2\xi^{qrp}_{121'}X^q_{\omega_c c}(\mathbf{r}_1,\mathbf{r}_2)V^{qr}_{cc}(\mathbf{r}_2)\left[X^c_{c\omega_c}(\mathbf{r}_2,\mathbf{r}_{1'}) + N^c_{c\omega_c}(\mathbf{r}_2,\mathbf{r}_{1'})\right]\Delta^r \\ &+ \sum_{qr\ge 2}\int d^3r_2\xi^{qrp}_{121'}\Delta^q X^c_{\omega_c c}(\mathbf{r}_1,\mathbf{r}_2)V^{qr}_{cc}(\mathbf{r}_2)\left[X^r_{c\omega_c}(\mathbf{r}_2,\mathbf{r}_{1'}) + N^r_{c\omega_c}(\mathbf{r}_2,\mathbf{r}_{1'})\right] \\ &+ N^p_{\rho\rho}(\mathbf{r}_1,\mathbf{r}_{1'}) + N^p_{\rho\omega_c}(\mathbf{r}_1,\mathbf{r}_{1'}) + N^p_{\omega_c\rho}(\mathbf{r}_1,\mathbf{r}_{1'})\,. \end{aligned} \tag{16}$$

The index $x(x')$ may assume the values $x(x') = d, e$ and denotes the exchange pattern and the type of correlation at a specific point. In general, we may have: d– and ω-vertices, if the point is reached by h– and ω-bonds, respectively, and does not belong to any exchange loop; an e–vertex if the point belongs to a closed exchange loop and it is reached by two e–bonds; c– and ω_c–vertices if the point belongs to an open exchange loop and it is reached by a single exchange line. The allowed (xx') combinations are: dd, de, ed. We indicate with $V^{qr}_{xx'}$ the vertex corrections, and with $\xi^{qrp}_{121'}$ the angular couplings. The expressions of these equations are all given in [15].

The above equations are derived in the FHNC/0 approximation, which does not include the contribution of the *elementary* diagrams. A detailed discussion of the importance of these diagrams and of the accuracy of the approximations used in solving the FHNC equations can be found in Refs. [42,43]. The FHNC/0 choice has been used in studies of the equation of state of nuclear matter [10], where it was found that the elementary diagrams contribution is not important because of the relatively low densities of the system. In finite nuclei elementary diagrams may play some role in the evaluation of the expectation value of potentials having strong exchange components [11]. In general, a measure of the relevance of the missing diagrams is provided by the accuracy of the sum rules of the one and two body densities.

The partial nodal functions, $N^p_{\omega x}$, are solutions of the integral equations:

$$N^p_{\omega x}(\mathbf{r}_1,\mathbf{r}_2) = \sum_{yy'}\sum_{qr}\int d^3r_3 \xi^{qrp}_{132} X^q_{\omega y}(\mathbf{r}_1,\mathbf{r}_3) V^{qr}_{yy'}(\mathbf{r}_3)\left[X^r_{y'x}(\mathbf{r}_3,\mathbf{r}_2)+N^r_{y'x}(\mathbf{r}_3,\mathbf{r}_2)\right] . \tag{17}$$

The $X^{p\geq 2}_{\omega x}$ links are

$$X^{p\geq 2}_{\omega d}(\mathbf{r}_1,\mathbf{r}_2) = h^p_\omega(\mathbf{r}_1,\mathbf{r}_2) h^c_\omega(\mathbf{r}_1,\mathbf{r}_2) - N^p_{\omega d}(\mathbf{r}_1,\mathbf{r}_2)\,, \tag{18}$$

$$X^p_{\omega e}(\mathbf{r}_1,\mathbf{r}_2) = h^c_\omega(\mathbf{r}_1,\mathbf{r}_2)\left[h^p_\omega(\mathbf{r}_1,\mathbf{r}_2) N^c_{\omega e}(\mathbf{r}_1,\mathbf{r}_2) + f^c(r_{12}) N^p_{\omega e}(\mathbf{r}_1,\mathbf{r}_2)\right] - N^p_{\omega e}(\mathbf{r}_1,\mathbf{r}_2)\,, \tag{19}$$

$$h^p_\omega(\mathbf{r}_1,\mathbf{r}_2) = f^p(r_{12}) + f^c(r_{12}) N^p_{\omega d}(\mathbf{r}_1,\mathbf{r}_2)\,, \tag{20}$$

and $h^c_\omega(\mathbf{r}_1,\mathbf{r}_2) = \exp\left[N^c_{\omega d}(\mathbf{r}_1,\mathbf{r}_2)\right]$. Moreover, the $N(X)^p_{xy}(\mathbf{r}_1,\mathbf{r}_2) = N(X)^p_{yx}(\mathbf{r}_2,\mathbf{r}_1)$ property holds. The central $X^c_{\omega x}$ links are defined in [27], and the X^p_{xy} and N^p_{xy} functions in [15].

For the $\omega_c c$–type nodals we have $N^p_{\omega_c c} = N^p_{\omega_c x} + N^p_{\omega_c \rho} + N^p_{\rho x} + N^p_{\rho\rho}$. $N^p_{\omega_c x}$ and $N^p_{\omega_c \rho}$ are solutions of

$$\begin{aligned} N^p_{\omega_c x}(\mathbf{r}_1,\mathbf{r}_2) = &\sum_{qr}\int d^3r_3 \xi^{qrp}_{132} X^q_{\omega_c c}(\mathbf{r}_1,\mathbf{r}_3) V^{qr}_{cc}(\mathbf{r}_3)\left[X^c_{cc}(\mathbf{r}_3,\mathbf{r}_2) + N^c_{xx}(\mathbf{r}_3,\mathbf{r}_2) + N^c_{\rho x}(\mathbf{r}_3,\mathbf{r}_2)\right]\Delta^r \\ &+ \sum_{qr\geq 2}\int d^3r_3 \xi^{qrp}_{132} \Delta^q X^c_{\omega_c c}(\mathbf{r}_1,\mathbf{r}_3) V^{qr}_{cc}(\mathbf{r}_3)\left[X^r_{cc}(\mathbf{r}_3,\mathbf{r}_2) + N^r_{xx}(\mathbf{r}_3,\mathbf{r}_2) + N^r_{\rho x}(\mathbf{r}_3,\mathbf{r}_2)\right] , \end{aligned} \tag{21}$$

$$\begin{aligned} N^p_{\omega_c \rho}(\mathbf{r}_1,\mathbf{r}_2) = &\sum_{qr}\int d^3r_3 \xi^{qrp}_{132} X^q_{\omega_c c}(\mathbf{r}_1,\mathbf{r}_3) V^{qr}_{cc}(\mathbf{r}_3)\left[-N_0(\mathbf{r}_3,\mathbf{r}_2) + N^c_{x\rho}(\mathbf{r}_3,\mathbf{r}_2) + N^c_{\rho\rho}(\mathbf{r}_3,\mathbf{r}_2)\right]\Delta^r \\ &+ \sum_{qr\geq 2}\int d^3r_3 \xi^{qrp}_{132} \Delta^q X^c_{\omega_c c}(\mathbf{r}_1,\mathbf{r}_3) V^{qr}_{cc}(\mathbf{r}_3)\left[N^r_{x\rho}(\mathbf{r}_3,\mathbf{r}_2) + N^r_{\rho\rho}(\mathbf{r}_3,\mathbf{r}_2)\right] . \end{aligned} \tag{22}$$

The equations for $N^p_{\rho x}$ and $N^p_{\rho\rho}$ are given in [15]. The links $X^{p\geq 2}_{\omega_c c}$ are

$$\begin{aligned} X^{p\geq 2}_{\omega_c c}(\mathbf{r}_1,\mathbf{r}_2) = &\, h^p_\omega(\mathbf{r}_1,\mathbf{r}_2) h^c_\omega(\mathbf{r}_1,\mathbf{r}_2)\left[N^c_{\omega_c c}(\mathbf{r}_1,\mathbf{r}_2) - N_0(\mathbf{r}_1,\mathbf{r}_2)\right] \\ &+ \left[f^c(r_{12}) h^c_\omega(\mathbf{r}_1,\mathbf{r}_2) - 1\right] N^p_{\omega_c c}(\mathbf{r}_1,\mathbf{r}_2)\,. \end{aligned} \tag{23}$$

Again, $X^c_{\omega_c c}$ is defined in [27].

The vertex corrections, ξ^c_ω, are discussed in [27] and $\Delta\xi^{op}_\omega$ is given by:

$$\begin{aligned} \Delta\xi^{op}_\omega(\mathbf{r}_1) = &\, U^{op}_\omega(\mathbf{r}_1) + \sum_{p\geq 2}\frac{A^p}{2}\int d^3r_2 \left\{X^p_{\omega d}(\mathbf{r}_1,\mathbf{r}_2) N^p_{\omega d}(\mathbf{r}_1,\mathbf{r}_2)\rho^c_1(\mathbf{r}_2)\right. \\ &+ \left.\left[X^p_{\omega d}(\mathbf{r}_1,\mathbf{r}_2) N^p_{\omega e}(\mathbf{r}_1,\mathbf{r}_2) + X^p_{\omega e}(\mathbf{r}_1,\mathbf{r}_2) N^p_{\omega d}(\mathbf{r}_1,\mathbf{r}_2)\right] C_d(\mathbf{r}_2)\right\} . \end{aligned} \tag{24}$$

ρ^c_1 (the Jastrow part of the one body density) and C_d are given in [15], and U^{op}_ω is obtained by eq.(2.12) of [27] with the substitutions $\rho^c_1 \to \rho_1 - \rho^c_1$ and $C_d \to C_d U^{op}_d$.

III. RESULTS FOR THE MOMENTUM DISTRIBUTION AND NATURAL ORBITS

In our work we used the Argonne v_8' NN potential. This model is based upon the v_{18} potential and it is constructed by considering only the first eight operator terms, up to the spin–orbit ones. It reproduces the isoscalar part of the full interaction, v_{18}, in the S, P and $^3D_1$ waves and the $^3D_1$–$^3S_1$ coupling. Argonne v_8' was introduced in Ref. [5] because its parametrization (simpler than that of other realistic potentials, since L^2 and $(L \cdot S)^2$ components are missing) allowed for a large simplification in the numerically involved quantum Monte Carlo calculations. The v_8' potential is slightly more attractive than v_{18}, and, for this reason, the strength of the associated repulsive part of the three–nucleon force (Urbana IX model) has been increased by 30% with respect to the original version. The results presented in this paper have been obtained with this hamiltonian (A8'+UIX model).

The correlation functions, $f^p(r)$, and the single particle functions, $\phi_\alpha(i)$, are the two ingredients necessary to construct the many–body wave function (2). We use a f_6 correlation, therefore, with respect to the structure of the hamiltonian, we neglect the spin–orbit components. The correlation is determined by minimizing the nuclear matter energy at the lowest order of the cluster expansion, considering the Fermi momentum, k_F, as one of the variational parameters. The resulting two–body Euler equations are solved with the *healing* conditions $f^1(r \geq d_1) = 1$, $f^{p>1}(r \geq d_p) = 0$, and requiring that the first derivatives vanish at $r = d_p$. Only two healing distances are introduced, d_c for the four central channels and d_t for the tensor ones, and they are variationally fixed. More details on this procedure are given in Ref. [14] for nuclear matter and in [15] for nuclei.

The single particle wave functions have been obtained by solving the single particle Schrödinger equation with a Woods–Saxon potential,

$$V_{WS}(r) = \frac{V_0}{1 + \exp\left[(r - R_0)/a_0\right]} \, . \tag{25}$$

A full minimization for the A8'+UIX model has been obtained in Ref. [13] and it has provided a binding energy per nucleon, B/A, of 5.48 MeV in ^{16}O and 6.97 MeV in ^{40}Ca, to be compared with the experimental values of 7.97 MeV (^{16}O) and 8.55 MeV (^{40}Ca). These differences are comparable with those obtained in nuclear matter at the empirical saturation density, ρ_{NM} =0.16 fm^{-3}, with the same hamiltonian. In fact, the FHNC/SOC nuclear matter energy per nucleon, E_{NM}, is E_{NM} =-10.9 MeV [13], against the empirical value of -16 MeV.

The nuclear root mean square radii (rms) were found to be 2.83 fm in ^{16}O and 3.66 fm in ^{40}Ca (the experimental radii are 2.73 fm and 3.48 fm, respectively). However, the one body densities at the variational minimum did not show a satisfactory agreement with the experimental ones. Moreover, shallow minima with respect to variations of the mean field parameters around the minimum itself were found in Ref. [13]. In particular, if one chooses a set of single particle wave functions which reproduces at best the empirical densities, the A8'+UIX model provided B/A=5.41 MeV in ^{16}O and B/A=6.64 MeV in ^{40}Ca, with rms(^{16}O)=2.67 fm and rms(^{40}Ca)=3.39 fm. Therefore, the density description has largely improved while the energy variations are kept within the accuracy of the FHNC/SOC scheme. The results presented in this paper have been obtained by means of this type of wave function, whose parameters are given in Table V of Ref. [13].

The one body densities generated by the FHNC/SOC scheme are shown in Fig. 1, where the solid lines give the densities obtained with the full correlation, the dot–dashed lines are those obtained with the Jastrow correlation (retaining only the p =1 component) and the dashed lines are the IPM densities. The effect of the operatorial correlation is large with respect to the Jastrow case, that is hardly distinguishable from the IPM one. The comparison with the experimental results has been presented in Ref. [13], where the proton densities are folded with the electromagnetic nucleon form factor.

The momentum distributions are given in Fig. 2. Again the solid and dot–dashed lines are the fully correlated and Jastrow results, respectively, while the IPM ones are shown as dashed lines. The squares are the VMC results [8] for ^{16}O obtained with the Argonne v_{14} [44] NN interaction.

The MD is normalized as:

$$1 \, = \, \frac{\nu}{(2\pi)^3} \int d^3k \, n(k) \, , \tag{26}$$

where ν is the spin–isospin degeneracy. For the Jastrow correlation this normalization is satisfied within the 0.2–0.3 % in both nuclei, while for the f_6 model the error is $\sim$3 % in ^{16}O and $\sim$2 % in ^{40}Ca, reflecting the approximations of the SOC approach.

In Fig. 3 the MD of ^{16}O (thin continuous line) and that of ^{40}Ca (thin dashed line) are compared with those of nuclear matter normalized as in (26) and calculated in FHNC/SOC framework by using the same interaction. It is worth noticing that the differences between the Jastrow and the f_6 correlations are similar in the infinite and finite systems and that the three cases show an analogous behavior at large momentum values. This momentum region is dominated by the short range structure of the nuclear wave function, which is heavily affected by the NN correlations. The effect appears to be, to a large extent, independent on the nucleus. A similar behavior was found in Ref. [8], where the comparison was made among the ^{4}He, ^{16}O and nuclear matter momentum distributions. With respect to the Jastrow estimates the non central, tensor correlations enhance the tails of the MDs by a factor 2–3 slightly smaller than the one found in Ref. [8], which is roughly $\sim$4. The difference may be understood in terms of the stronger tensor force of the Argonne v_{14} potential adopted in that reference.

A more demanding sum rule for $n(k)$ than that expressed by eq.(26) can be obtained from the kinetic energy, T. The kinetic energy per particle can be evaluated via the MD as:

$$\frac{T}{A} = \frac{\hbar^2}{2m}\frac{\nu}{(2\pi)^3}\int d^3k\, k^2 n(k) \equiv T_{MD}\,. \tag{27}$$

The value of T/A can also be computed in the FHNC/SOC framework (T_{FHNC}), for example by means of the Jackson-Feenberg identity, as it has been done in Ref. [13] for the A8'+UIX model. The differences between T_{MD} and T_{FHNC} are a severe measure of the importance of the approximations made in the cluster expansion. For the Jastrow cases the relative disagreement, $\delta T = |T_{MD} - T_{FHNC}|/T_{FHNC}$, is $< 5\%$ (T_{MD}=20.52 MeV and T_{FHNC}=19.57 MeV in ^{16}O and T_{MD}=22.98 MeV and T_{FHNC}=22.05 MeV in ^{40}Ca). In the f_6 model we obtained T_{MD}=29.42 MeV, T_{FHNC}=32.64 MeV and δT =9% in ^{16}O and T_{MD}=36.63 MeV, T_{FHNC}=38.15 MeV and δT =9.6% in ^{40}Ca. This larger disagreement is due to the SOC truncation. The T_{MD} value is largely influenced by the behavior of the momentum distribution at high k–values. The contribution of the k >4 fm^{-1} tail has been evaluated by an exponential extrapolation of the computed MD. As a check of the numerical accuracy, we have verified that T_{MD} coincides with T_{FHNC} for the IPM.

The NO and their occupation numbers are obtained by diagonalizing the OBDM:

$$\rho_1(\mathbf{r}_1, \mathbf{r}_{1'}) = \sum_\alpha n_\alpha \phi^{NO}_\alpha(\mathbf{r}_1)^\dagger \phi^{NO}_\alpha(\mathbf{r}_{1'})\,, \tag{28}$$

We treat spherical nuclei in ls single particle coupling, saturated in both spin and isospin. For this reason the spin–isospin part of eq. (12) provides the degeneracy ν=4. Because of the spherical symmetry the function $N(\mathbf{r}_1, \mathbf{r}_{1'})$ of eq. (12) can be expanded in multipoles, and we obtain for the OBDM:

$$\rho_1(\mathbf{r}_1, \mathbf{r}_{1'}) = \nu \sum_l \frac{2l+1}{4\pi} P_l(\cos\theta_{11'})\rho_l(r_1, r_{1'})\,, \tag{29}$$

where $P_l(x)$ represents the Legendre polinomials and $\theta_{11'}$ is the angle between $\mathbf{r}_1$ and $\mathbf{r}_{1'}$.

Exploiting again the spherical symmetry, the natural orbitals can be written as:

$$\phi^{NO}_{\alpha=nlm}(\mathbf{r}) = \phi^{NO}_{nl}(r)\, Y_{lm}(\hat{r})\chi_{\sigma\tau}\,, \tag{30}$$

where we indicate with $Y_{lm}(\hat{r})$ the spherical harmonics and with $\chi_{\sigma\tau}$ the spin–isospin part of the wave function. The normalization condition is:

$$1 = \int r^2\, dr |\phi^{NO}_{nl}(r)|^2\,. \tag{31}$$

Therefore we obtain:

$$\rho_l(r_1, r_{1'}) = \nu \sum_n n_{nl}\, \phi^{NO}_{nl}(r_1)\, \phi^{NO}_{nl}(r_{1'})\,, \tag{32}$$

The nl–natural orbitals and their occupations have been obtained by direct diagonalization of the matrix $\rho_l(r_1, r_{1'})$.

The first three NO of ^{16}O and ^{40}Ca, calculated for the three lowest l–values are shown in Figs. 4 and 5. In Table I the occupation numbers of the various NO for Jastrow and f^6 correlations are presented.

The effect of the correlations on the shell model orbitals are mainly visible in the short range part of the $1s$ state, making this NO more localized than its IPM counterpart. The shape of the other IPM states is barely influenced by the correlations. The occupation of the NO corresponding to the shell model ones is depleted by as much as 22% (the $2s$ state in ^{40}Ca). In contrast, the mean field unoccupied states become sizeably populated. The two effects are largely due to the tensor part of the correlation operator.

It was pointed out in Ref. [45], that when there is more than one occupied state in the IPM for a given l–value (as for the s–states in ^{40}Ca), then the natural orbitals may be qualitatively different from the IPM ones. In fact, any orthogonal combination of the mean field orbitals does not change the corresponding density matrix. New mean field s–orbitals, $\hat{\phi}_{ns}$, consistent with $\rho_{IPM}(\mathbf{r}_1, \mathbf{r}_{1'})$, can be obtained in ^{40}Ca by the transformations:

$$\hat{\phi}_{1s}(\mathbf{r}) = \cos(\alpha)\phi_{1s}(\mathbf{r}) + \sin(\alpha)\phi_{2s}(\mathbf{r}) \, , \tag{33}$$

$$\hat{\phi}_{2s}(\mathbf{r}) = \cos(\alpha)\phi_{2s}(\mathbf{r}) - \sin(\alpha)\phi_{1s}(\mathbf{r}) \, , \tag{34}$$

for any choice of the angle α. The IPM orbitals of the l=0 panel in Fig. 5 are obtained by a numerical diagonalization of the one–body density matrix and roughly correspond to $\cos(\alpha) = .8$.

The ^{16}O natural orbits have been evaluated in Ref. [32] within a Green function approach and using the one–boson–exchange Bonn B potential of Ref. [46]. The authors find the n =1 NO more populated than the CBF ones for the occupied states in the shell model approach (l =0, 1), and, consequently, lower occupations for all the remaining orbitals. Specifically, the n=1 Green function results are: n_{1s}=.921, n_{1p}=.941 and n_{1d}=.017. The $1p$ ($1d$) occupation number has been taken as the average of the $1p_{1/2}$ and $1p_{3/2}$ ($1d_{3/2}$ and $1d_{5/2}$) orbitals given in the reference. The discrepancies are probably to be ascribed more to the different potentials adopted, rather than to the methodologies. The A8'+UIX model induces stronger correlation, so giving a larger depletion of the lowest NO. This effect was also found in the study of ^{3}He atomic drops of Ref. [45], where the strong repulsive interaction between the ^{3}He atoms depletes the shell model occupations by 15–46 %. The CBF total occupation numbers in the l–th orbitals for ^{16}O and ^{40}Ca with different correlations (f_6, f_4, without tensor components, and Jastrow, J) are given in Table II, together with the ^{16}O Green function ones from Ref. [32]. It appears clearly that the longer ranged tensor correlations are responsible of most of the deoccupation of the shell model natural orbitals in favour of the higher ones.

Fig. 6 presents a comparison between the ^{16}O NO in FHNC/SOC and in the lowest order approximation. This approach consists in truncating the cluster expansion at the first order in the dynamical correlation lines [47,48,29] and it has achieved a certain degree of popularity because of its simplicity. The approximation provides a good description of the n=1 NO corresponding to the occupied shell model states, but it fails to reproduce the other ones.

To conclude this section, we give in Fig. 7 the partial wave decomposition of the correlated and IPM one body densities in terms of their natural orbits.

IV. QUASI HOLE STATES AND SINGLE PARTICLE OVERLAP FUNCTIONS

A considerable amount of information on the properties of the single nucleon in the nuclear medium can be deduced from $(e, e'p)$ reactions. These experiments have been analyzed to extract the quasihole function, $\psi_h(\mathbf{r})$, given by the overlap between the A–body ground–state and the (A-1)–body hole state of the residual system.

In a fixed center reference frame, the QH function is defined as:

$$\psi_h(x) = \sqrt{A}\frac{\langle\Psi_h(A-1)|\delta(x-x_A)|\Psi_0(A)\rangle}{\langle\Psi_h(A-1)|\Psi_h(A-1)\rangle^{1/2}\langle\Psi_0(A)|\Psi_0(A)\rangle^{1/2}} \, , \tag{35}$$

In doubly closed shell nuclei in the ls coupling scheme it is possible to separate the radial dependence of the QH function from the angular, spin and isospin ones, as:

$$\psi_h(x) = \psi_h(r)Y_{lm}(\hat{r})\chi_{\sigma\tau} = \psi_h(r)\mathcal{Y}_{lm\sigma\tau}(\hat{r}) \, . \tag{36}$$

In the IPM, the QH overlaps are simply the shell model functions and $\psi_h^{IPM}(r) = R_{h=nl}(r)$, where $R_h(r_i)$ is the radial part of $\phi_\alpha(i)$.

In CBF theory $\Psi_0(1,2...A)$ is given by (2) and

$$\Psi_h(1,2...A-1) = G(1,2...A-1)\Phi_h(1,2...A-1), \tag{37}$$

where $\Phi_h(1,2...A-1)$ is a Slater determinant obtained by removing from $\Phi_0(1,2...A)$ a nucleon in the state h.

In order to develop a cluster expansion for $\psi_h(r)$ it is convenient to rearrange (35) as:

$$\psi_h(r) = \mathcal{X}_h(r)\mathcal{N}_h^{1/2} \, , \tag{38}$$

where

$$\mathcal{X}_h(r) = \sqrt{A}\frac{\langle\Psi_h(A-1)|\mathcal{Y}_{lm\sigma\tau}(\hat{r},\sigma,\tau)\delta(\mathbf{r}-\mathbf{r}_A)|\Psi_0(A)\rangle}{\langle\Psi_h(A-1)|\Psi_h(A-1)\rangle} \, , \tag{39}$$

and

$$\mathcal{N}_h = \frac{\langle \Psi_h(A-1)|\Psi_h(A-1)\rangle}{\langle \Psi_0(A)|\Psi_0(A)\rangle} \,. \tag{40}$$

Cluster expansions are used to compute $\mathcal{X}_h$ and $\mathcal{N}_h$, along the lines followed in Ref. [50] to evaluate the overlap matrix elements in the CBF approach to the nuclear matter spectral function.

The expansion for $\mathcal{X}_h$ is linked, in the sense that disconnected diagrams in the numerator are exactly canceled by those coming from the denominator. Its FHNC/0 expression, when only Jastrow correlations are considered, is:

$$\begin{aligned}\mathcal{X}^J_{nl}(r) = \xi^{nl}_\omega(r) \Big\{ R_{nl}(r) + \int d^3r_1 R_{nl}(r_1) P_l(\cos\theta) \left[g^{nl}_{\omega d}(\mathbf{r},\mathbf{r}_1) C^{nl}_d(\mathbf{r}_1) \right. \\ \times \left. \left(-\rho^{nl}_{IPM}(\mathbf{r},\mathbf{r}_1) + N^{nl}_{\omega_c c}(\mathbf{r},\mathbf{r}_1) \right) + \rho^{nl}_{IPM}(\mathbf{r},\mathbf{r}_1) - N^{nl}_{\omega_c \rho}(\mathbf{r},\mathbf{r}_1) - N^{nl}_{\rho\rho}(\mathbf{r},\mathbf{r}_1) \right] \Big\} \,,\end{aligned} \tag{41}$$

where θ is the angle betwen $\mathbf{r}$ and $\mathbf{r}_1$, and ρ^h_{IPM} is the A-1 one–body density matrix in the independent particle model,

$$\rho^h_{IPM}(\mathbf{r}_1,\mathbf{r}_{1'}) = \sum_{\alpha\neq h} \phi^\dagger_\alpha(1)\phi_\alpha(1') \,. \tag{42}$$

In $\mathcal{N}_h$ only those diagrams from the denominator containing explicitely the h–orbital survive. The Jastrow, FHNC/0 expression is:

$$\begin{aligned}[\mathcal{N}^J_{nl}]^{-1} = \int d^3r C^{nl}_d(\mathbf{r}) \Big\{ |\phi_{nl}(\mathbf{r})|^2 + \int d^3r_1 \phi^\dagger_{nl}(\mathbf{r})\phi_{nl}(\mathbf{r}_1) \left[g^{nl}_{dd}(\mathbf{r},\mathbf{r}_1) C^{nl}_d(\mathbf{r}_1) \right. \\ \times \left. \left(-\rho^{nl}_{IPM}(\mathbf{r},\mathbf{r}_1) + N^{nl}_{cc}(\mathbf{r},\mathbf{r}_1) \right) + \rho^{nl}_{IPM}(\mathbf{r},\mathbf{r}_1) - N^{nl}_{x\rho}(\mathbf{r},\mathbf{r}_1) - N^{nl}_{\rho\rho}(\mathbf{r},\mathbf{r}_1) \right] \Big\} \,.\end{aligned} \tag{43}$$

The FHNC quantities entering $\mathcal{X}^J_{nl}$ and $\mathcal{N}^J_{nl}$ correspond to those given in Refs. [27,11], but evaluated with the A-1 densities, $\rho^h_{IPM}(\mathbf{r}_1,\mathbf{r}_{1'})$ and $\rho^h_{1,IPM}(\mathbf{r}_1) = \sum_{\alpha\neq h} |\phi_\alpha(1)|^2$. In absence of correlations, $\mathcal{X}^J_{nl}(r) \to R_{nl}(r)$ and $\mathcal{N}^J_{nl} \to 1$.

The FHNC/SOC expressions of $\mathcal{X}_{nl}$ and $\mathcal{N}_{nl}$, with operatorial correlations, are given in the Appendix.

The quasihole normalization gives the spectroscopic factor, S_h,

$$S_h = \int r^2 dr \psi^2_h(r) \,. \tag{44}$$

In a fixed center IPM (as the one we adopt as model function), $S^{IPM}_h = 1$. Center of mass (cm) corrections are sources of deviation. In the harmonic oscillator model they enhance S_h for the valence hole states (those with the largest oscillator quantum number, N_v) by a $[A/(A-1)]^{N_v}$ factor [49]. As a consequence, the cm–corrected $1p$–shell spectroscopic factor of ^{16}O is $S^{HO}_{1p,cm} = 16/15 \sim 1.07$, while the average between the $2s$ and $1d$ states in ^{40}Ca is $S^{HO}_{2s/1d,cm} = (40/39)^2 \sim 1.05$. More realistic Woods–Saxon orbitals do not allow for an analytical treatment of cm effects, which have to be computed numerically. It has been found that in ^{16}O the $1p$ WS spectroscopic factor practically coincides with the HO one [34].

The correlated spectroscopic factors (without cm corrections) in ^{16}O and ^{40}Ca are given in Table III for f_6, f_4 and Jastrow correlation factors. Jastrow correlations marginally reduce S_h (at most 3%). Central spin–isospin correlations (f_4 model) also provide a few percent depletion in the valence states, whereas the tensor ones (f_6) give most of the reduction bringing S_{1p} in ^{16}O to 0.90 and S_{2s} and S_{1d} in ^{40}Ca to 0.86 and 0.87, respectively. The $1p$ CBF ^{16}O result is in complete agreement with the VMC estimate [34]. The influence of the operatorial correlations is much larger in the low lying states, whose spectroscopic factors are drastically reduced by both central and tensor components: S_{1s} in ^{16}O is 0.70, S_{1p} and S_{1s} in ^{40}Ca are 0.58 and 0.55, respectively. An analogous behavior was found by Benhar [51], who first used low order cluster expansions to estimate S_h in the $^{12}\mathrm{C}(e,e'p)^{11}\mathrm{B}$ reaction with state dependent correlations and found S_{1p}=0.55 and S_{1s}=0.25.

Results similar to those presented in this paper have been obtained in Refs. [36,37], where the ^{16}O S_{1p} has been extracted by several models of OBDM [35]. In particular, in both references it is confirmed that correlation effects on this spectroscopic factor are dominated by tensor components. The lowest order truncation of the OBDM cluster expansion adopted in Ref. [37] provides $S_{1p,LO} \sim 0.90$, in agreement with the FHNC/SOC results. However, the authors find $S_{1s,LO} \sim 0.86$, in contrast with the 0.70 FHNC/SOC value. The origin of this large difference may lay in the lowest order approximation in the cluster expansion. This issue is presently object of investigation.

The latest experimental extraction of S_p from the $^{16}\mathrm{O}(e,e'p)^{15}\mathrm{N}$ reaction [52] reports $S_{p_{1/2}}$=0.61 for the $1/2^-$ ground state in ^{15}N and $S_{p_{3/2}}(6.32)$=0.53 for the lowest $3/2^-$ state at 6.32 MeV. This state exhibits 87% of the total $S_{p_{3/2}}$ strength, that is fragmented over three states at 6.32, 9.93 and 10.70 MeV. So, the total $S_{p_{3/2}}$ may be estimated to be $S_{p_{3/2}}$=0.53/0.87=0.61 [34].

A corresponding situation is met in the $^{40}\mathrm{Ca}(e,e'p)^{39}\mathrm{K}$ reaction [23], where the transition to the $1d_{3/2}$ ground state gives $S_{d_{3/2}}$ ∼0.61±0.07, while the FHNC/SOC value is S_d =0.87. The ^{40}Ca spectroscopic factors have been computed by the low order cluster expansion of the OBDM in a Jastrow model in Ref. [53]. The results are consistenly lower than the FHNC ones, reported in the 5th column of Table III. For instance, $S_{2s,LO}$=0.95 and $S_{1d,LO}$=0.91, whereas $S_{2s,FHNC}$=0.98 and $S_{1d,FHNC}$=0.97. The discrepancies are probably to be ascribed to the approximation used in the reference to evaluate the OBDM.

The squared quasihole functions are shown in Fig.8. The solid and dot–dashed lines give the full f_6 and Jastrow results, respectively. The IPM estimates are given as dashed lines. The spin–isospin dependent correlations are the main responsible for the quenching of the IPM QH functions, consistently with the spectroscopic factor values, whereas the Jastrow components have little effect on the overlaps, and mostly in the valence states. In Ref. [54] a Woods–Saxon potential was used to generate a single–particle wave function to fit the $^{16}\mathrm{O}(e,e'p)^{15}\mathrm{N}$ cross section to the 6.32 MeV state with $S_{p_{3/2}}(6.32)$=0.53. $|\psi_{WS}|^2$ is shown in the $|\psi_{1p}|^2$–^{16}O panel as stars. In order to give a meaningful comparison, we rescale $|\psi_{1p,FHNC}|^2$ by the factor 0.53/0.90. The result is shown as a dot–dashed line and it is in nice agreement with the empirical estimate.

The knowledge of $\psi_h(r)$ may give access to the cross sections. However, both Coulomb distortion and final state interactions should be properly accounted for, by evaluating the Fourier transorm of a distorted overlap [55], to perform a quantitative comparison with the experiments. Work in this direction is in progress. In this paper we limit ourselves to give in Fig.9 the squared Fourier transform of some quasihole functions,

$$\psi_h(k) = \int d^3r e^{i\mathbf{k}\cdot\mathbf{r}}\ \psi_h(r)\,. \tag{45}$$

In the valence states ($1p$ for ^{16}O and $1d$ for ^{40}Ca) short range correlations slightly deplete $|\psi_h(k)|^2$ at large momenta with respect to the IPM. The effect of the correlations is more visible in the two low lying states given in the figure ($1s$ for both nuclei). For instance, in the $1s$ ^{16}O case Jastrow correlations are effective at large momenta only, beyond the first IPM zero; instead, tensor correlations modify both the low and large momenta behaviors. The same effect is found in ^{40}Ca.

V. SUMMARY AND CONCLUSIONS

In this work we have calculated one-body density matrices, momentum distributions, natural orbits and quasi-hole states of ^{16}O and ^{40}Ca using the FHNC/SOC resummation technique, which allows for using realistic interactions and state dependent correlations. The calculations have been done with the Argonne v_8' two–nucleon potential plus the Urbana IX three–nucleon interaction, together with a set of single particle wave functions fixed to reproduce at best the empirical charge distributions of the two nuclei. The parameters of the correlation have been chosen to minimize the binding energies. Using these wave functions, we have investigated the role of the correlations on the quantitites above mentioned.

Our density and momentum distributions confirm some well known results. Short-range correlations have small effects on the density distributions and mainly around the center of the nucleus. On the contrary, the high momentum tail of the momentum distribution is dominated by the correlations. We have pointed out that the tensor correlations enhance these tail by a factor 3-4 with respect to the results obtained with Jastrow correlations.

The tensor part of the correlation is important in the calculation of the occupation probabilities of the natural orbits. The effect of reducing the occupation of the level below the Fermi surface and enhancing those which lies above is amplified by the tensor terms of the correlation. We found that the shape of the natural orbits below the Fermi surface is rather similar to that of the corresponding single particle wave functions.

The natural orbits have also beeen calculated within a lowest-order computational scheme. The agreement with the orbit below the Fermi surface is excellent. The lowest order calculation produces orbits above the Fermi surface with completely different shape with respect to those obtained by the full calculation.

Tensor correlations play a relevant role also for the evaluation of the overlap functions and spectroscopic factors. The correlated overlap functions are close to the corresponding single particle wave functions if only Jastrow correlations are used. The inclusion of the tensor correlations strongly modifies their shapes. This behavior is also clear from the analysis of the spectroscopic factors. The depletion of a few percent, with respect to one, obtained with Jastrow correlations, becomes of about 10-15% for the valence levels and 30-45% for the deeply lying ones.

In spite of this noticeable reduction, the FHNC/SOC approach in ^{16}O is still unable to reproduce the empirical $S_{p_{3/2}}$ spectroscopic factor extracted from $(e,e'p)$ reactions. A similar behavior was found in Ref. [56] for nuclear matter, where the variational FHNC/SOC calculation of the one–hole strength, $Z(e)$, around the Fermi level provided $Z_v(e \sim e_F)$ ∼0.88, mostly due to tensor correlations. Second order perturbative corrections in a correlated basis, obtained by considering the contribution of two–hole one–particle, $(2h-1p)$, correlated states, $\Psi_{2h-1p} = G\Phi_{2h-1p}$, were found to bring the strength to $Z_{CBF}(e \sim e_F) \sim 0.70$, so explaining almost half of the discrepancy with the empirical ^{208}Pb spectroscopic factor, $Z(^{208}Pb) \sim 0.5-0.6$. The remaining part of the difference was attributed to the coupling of the single particle waves to the collective low-lying surface vibrations, not reproducible in infinite nuclear matter. We expect that in finite nuclei, the inclusion of correlated $2h-1p$ corrections can take into account also great part of the coupling with surface vibrations.

AKNOWLEDGMENTS

This work has been partially supported by MURST through the *Progetto di Ricerca di Interesse Nazionale: Fisica teorica del nucleo atomico e dei sistemi a molticorpi.*

APPENDIX

We present in this Appendix the FHNC/SOC expressions for the $\mathcal{X}_{nl}$ and $\mathcal{N}_{nl}$ functions:

$$\begin{aligned}\mathcal{X}_{nl}(r) = {} & \mathcal{X}^J_{nl}(r)\left[1+\Delta\xi^{op,nl}_{\omega}(r)\right] + \xi^{nl}_{\omega}(r)\int d^3r_1 R_{nl}(r_1)P_l(\hat{r},\hat{r}_1) \\ & \times \Big\{ g^{c,nl}_{\omega d}(\mathbf{r},\mathbf{r}_1) C^{nl}_d(\mathbf{r}_1) U^{op,nl}_d(\mathbf{r}_1)\left(-\rho^{nl}_{IPM}(\mathbf{r},\mathbf{r}_1)+N^{c,nl}_{\omega_c c}(\mathbf{r},\mathbf{r}_1)\right) \\ & + \sum_{p\geq 2}\Big[h^{p,nl}_{\omega}(\mathbf{r},\mathbf{r}_1) h^{c,nl}_{\omega}(\mathbf{r},\mathbf{r}_1) C^{nl}_d(\mathbf{r}_1)\left(-\rho^{nl}_{IPM}(\mathbf{r},\mathbf{r}_1)+N^{c,nl}_{\omega_c c}(\mathbf{r},\mathbf{r}_1)\right) \\ & + \; g^{c,nl}_{\omega d}(\mathbf{r},\mathbf{r}_1) C^{nl}_d(\mathbf{r}_1) N^{p,nl}_{\omega_c c}(\mathbf{r},\mathbf{r}_1) - N^{p,nl}_{\omega_c \rho}(\mathbf{r},\mathbf{r}_1) - N^{p,nl}_{\rho\rho}(\mathbf{r},\mathbf{r}_1)\Big] A^p\Delta^p \Big\} \;, \end{aligned} \tag{46}$$

$$\begin{aligned}[\mathcal{N}_{nl}]^{-1} = {} & \int d^3r C^{nl}_d(\mathbf{r})\left[1+U^{op,nl}_d(\mathbf{r})\right]\Big\{ |\phi_{nl}(\mathbf{r})|^2 + \int d^3r_1 \phi^{\dagger}_{nl}(\mathbf{r})\phi_{nl}(\mathbf{r}_1) \\ & \times \left[g^{nl}_{dd}(\mathbf{r},\mathbf{r}_1) C^{nl}_d(\mathbf{r}_1)\left(-\rho^{nl}_{IPM}(\mathbf{r},\mathbf{r}_1)+N^{nl}_{cc}(\mathbf{r},\mathbf{r}_1)\right)\right. \\ & \left. + \; \rho^{nl}_{IPM}(\mathbf{r},\mathbf{r}_1) - N^{nl}_{x\rho}(\mathbf{r},\mathbf{r}_1) - N^{nl}_{\rho\rho}(\mathbf{r},\mathbf{r}_1)\right]\Big\} \\ & + \int d^3r C^{nl}_d(\mathbf{r})\int d^3r_1 \phi^{\dagger}_{nl}(\mathbf{r})\phi_{nl}(\mathbf{r}_1) \\ & \times \Big\{ g^{c,nl}_{dd}(\mathbf{r},\mathbf{r}_1) C^{nl}_d(\mathbf{r}_1) U^{op,nl}_d(\mathbf{r}_1)\left(-\rho^{nl}_{IPM}(\mathbf{r},\mathbf{r}_1)+N^{c,nl}_{cc}(\mathbf{r},\mathbf{r}_1)\right) \\ & + \sum_{p\geq 2}\Big[h^{p,nl}(\mathbf{r},\mathbf{r}_1) h^{c,nl}(\mathbf{r},\mathbf{r}_1) C^{nl}_d(\mathbf{r}_1)\left(-\rho^{nl}_{IPM}(\mathbf{r},\mathbf{r}_1)+N^{c,nl}_{cc}(\mathbf{r},\mathbf{r}_1)\right) \\ & + \; g^{c,nl}_{dd}(\mathbf{r},\mathbf{r}_1) C^{nl}_d(\mathbf{r}_1) N^{p,nl}_{cc}(\mathbf{r},\mathbf{r}_1) - N^{p,nl}_{x\rho}(\mathbf{r},\mathbf{r}_1) - N^{p,nl}_{\rho\rho}(\mathbf{r},\mathbf{r}_1)\Big] A^p\Delta^p \Big\} \;. \end{aligned} \tag{47}$$

[1] J. G. Zabolitzky and W, Ey, Phys. Lett. B **76**, 527 (1978); O. Bohigas and S. Stringari, Phys. Lett. B **95**, 9 (1980); M. Dal Rì, S. Stringari and O. Bohigas, Nucl. Phys. A **376**, 81 (1982); F. Dellagiacoma, G. Orlandini and M. Traini, Nucl. Phys. A **393**, 95 (1983); M. Jaminon, C, Mahaux and H. Ngô, Nucl. Phys. A **473**, 509 (1987).

[2] A. N. Antonov, P. E. Hodgson and I. Zh. Petkov *Nucleon momentum and density distributions* (Clarendon Press, Oxford, 1988).

[3] G. van der Steenhoven and P. K. A. de Witt Huberts, in *Modern Topics in Electron Scattering*, edited by B. Frois and I. Sick (World Scientific, Singapore, 1991), p.510.
[4] R. B. Wiringa, S. C. Pieper, J. C. Carlson, and V. R. Pandharipande, nucl-th/0002022.
[5] B. S. Pudliner, V. R. Pandharipande, J. Carlson, S. C. Pieper, and R. B. Wiringa, Phys. Rev. C **56**, 1720 (1997).
[6] C. R. Chen, G. L. Payne, J. L. Friar, and B. F. Gibson, Phys. Rev. C **33**, 1740 (1986); A. Stadler, W. Glöckle, and P. U. Sauer, Phys. Rev. C **44**, 2319 (1991).
[7] A. Kievsky, M. Viviani, and S. Rosati, Nucl. Phys. A **551**, 241 (1993).
[8] S. C. Pieper, R. B. Wiringa, and V. R. Pandharipande, Phys. Rev. C **46**, 1741 (1992).
[9] J. H. Heisenberg and B. Mihaila, Phys. Rev. C **59**, 1440 (1999).
[10] R. B. Wiringa, V. Ficks, and A. Fabrocini, Phys. Rev. C **38**, 1010 (1988).
[11] G. Co', A. Fabrocini, S. Fantoni, and I. E. Lagaris, Nucl. Phys. A **549**, 439 (1992).
[12] F. Arias de Saavedra, G. Co', A. Fabrocini, and S. Fantoni, Nucl. Phys. A **605**, 359 (1996).
[13] A. Fabrocini, F. Arias de Saavedra, and G. Co', Phys. Rev. C **61**, 044302 (2000).
[14] V. R. Pandharipande and R. B. Wiringa, Rev. Mod. Phys. **51**, 821 (1979).
[15] A. Fabrocini, F. Arias de Saavedra, G. Co', and P. Folgarait, Phys. Rev. C **57**, 1668 (1998).
[16] C. J. G. Onderwater et al. Phys. Rev. Lett. **78**, 4893 (1997); Phys. Rev. Lett. **81**, 2213 (1998); R. Starink et al. Phys. Lett. B **474**, 33 (2000).
[17] P. K. A. de Witt Huberts, J. Phys. G **16**, 507 (1990).
[18] C.E. Hyde-Wright *et al.*,Phys. Rev. C **35**, 880 (1987); J. E. Wise *et al.*, Phys. Rev. C **31**, 1699 (1985); J.P. Connelly *et al.*, Phys. Rev. C **45**, 2711 (1992).
[19] J.M. Cavedon *et al.*, Phys. Rev. Lett. **49**, 978 (1982).
[20] C. Papanicolas, in *Nuclear Structure at high spin, excitation and momentum transfer*, H. Nann ed., (American Institute of Physics, New York 1986), p. 110.
[21] C. Mahaux and R. Sartor, Adv. Nucl. Phys. **20**, 1 (1991).
[22] J. J. Kelly, Adv. Nucl. Phys. **23**, 75 (1996).
[23] L. Lapikás, Nucl. Phys. A **553**, 297c (1993).
[24] S. Fantoni, Nuovo Cimento A **44**, 178 (1978).
[25] S. Fantoni and V. R. Pandharipande, Nucl. Phys. A **427**, 59 (1983).
[26] O. Benhar, A. Fabrocini, and S. Fantoni, Nucl. Phys. A **550**, 201 (1992).
[27] G. Co', A. Fabrocini, and S. Fantoni, Nucl. Phys. A **568**, 73 (1994).
[28] O. Benhar, C. Ciofi degli Atti, S. Liuti, and G. Salmè, Phys. Lett. B **177**, 135 (1986).
[29] F. Arias de Saavedra, G. Co', and M.M. Renis, Phys. Rev. C **55**, 673 (1997).
[30] Ch. E. Moustakidis, and S. E. Massen, Phys. Rev. C **62**, 034318 (2000).
[31] S. Stringari, M. Traini, and O. Bohigas, Nucl. Phys. A **516**, 33 (1990).
[32] A. Polls, H. Müther, and W. H. Dickhoff, Nucl. Phys. A **594**, 117 (1995).
[33] L. Lapikás, J. Wesseling, and R.B. Wiringa, Phys. Rev. Lett. **82**, 4404 (1999).
[34] D. Van Neck, M. Waroquier, A. E. L. Dieperink, S. C. Pieper, and V. R. Pandharipande, Phys. Rev. C **57**, 2308 (1998).
[35] D. Van Neck, M. Waroquier, and K. Heyde, Phys. Lett. B **314**, 255 (1993).
[36] M. K. Gaidarov, K. A. Pavlova, A. N. Antonov, M. V. Stoitsov, S. S. Dimitrova, M. V. Ivanov, and C. Giusti, Phys. Rev. C **61**, 014306 (1999).
[37] D. Van Neck, L. Van Daele, and M. Waroquier, Phys. Rev. C **56**, 1398 (1997).
[38] K. Amir–Azimi–Nili, J. M. Udias, H. Müther, L. D. Skouras, and A. Polls, Nucl. Phys. A **625**, 633 (1997).
[39] R. A. Arndt, L. D. Roper, R. L. Workman, and M. W. McNaughton, Phys. Rev. D **45**, 3995 (1992).
[40] V. G. J. Stoks, R. A. M. Klomp, M. C. M. Rentmeester, and J. J. DeSwart, Phys. Rev. C **48**, 792 (1993).
[41] R. B. Wiringa, V. G. J. Stoks, and R. Schiavilla, Phys. Rev. C **51**, 38 (1995).
[42] A. Fabrocini, V. R. Pandharipande, Q. N. Usmani, Nuovo Cimento D **5**, 469 (1992).
[43] M. Viviani, E. Buendìa, A. Fabrocini, and S. Rosati, Nuovo Cimento D **8**, 561 (1986).
[44] R. B. Wiringa, R. A. Smith, and T. L. Ainsworth, Phys. Rev. C **29**, 1207 (1984).
[45] D. S. Lewart, V. R. Pandharipande, and S. C. Pieper, Phys. Rev. B **37**, 4950 (1988).
[46] R. Machleidt, Adv. Nucl. Phys. **19**, 1 (1989).
[47] M. V. Stoitsov, A. N. Antonov and S. S. Dimitrova, Z. Phys. A **345** (1993) 345; Phys. Rev. C **47** R455 (1993); Phys. Rev. C **48** 74 (1993).
[48] D. Van Neck, L. Van Daele, Y. Dewulf and M. Waroquier, Phys. Rev. C **56**, 1398 (1997).
[49] A. E. L. Dieperink, and T. de Forest, Phys. Rev. C **10**, 543 (1974).
[50] O. Benhar, A. Fabrocini, and S. Fantoni, Nucl. Phys. A **505**, 267 (1989).
[51] O. Benhar, in *Research Program at CEBAF (II). Report of the 1986 Summer Study Group*, CEBAF, 501 (1986).
[52] M. Leuscher *et al.*, Phys. Rev. C **49**, 955 (1994).
[53] M. V. Stoitsov, S. S. Dimitrova, and A. N. Antonov, Phys. Rev. C **53**, 1254 (1996).
[54] M. Radici, S. Boffi, S. C. Pieper, and V. R. Pandharipande, Phys. Rev. C **50**, 3010 (1994).
[55] O. Benhar, N. N. Nikolaev, J. Speth, A. A. Usmani, and B. G. Zakharov, Nucl. Phys. A **673**, 241 (2000).

[56] O. Benhar, A. Fabrocini and S. Fantoni, Phys. Rev. C **41**, R24 (1990).

TABLE I. Occupation numbers of the nl–th natural orbits for ^{16}O and ^{40}Ca in CBF, with the f_6 and Jastrow correlation models.

nl	$n_{nl}(f_6;^{16}\mathrm{O})$	$n_{nl}(\mathrm{J};^{16}\mathrm{O})$	$n_{nl}(f_6;^{40}\mathrm{Ca})$	$n_{nl}(\mathrm{J};^{40}\mathrm{Ca})$
$1s$	0.858	0.960	0.864	0.952
$2s$	0.019	0.005	0.780	0.962
$3s$	0.010	0.002	0.052	0.002
$4s$	0.005	0.001	0.013	0.001
$1p$	0.919	0.980	0.841	0.949
$2p$	0.021	0.004	0.024	0.009
$3p$	0.011	0.003	0.016	0.006
$1d$	0.025	0.006	0.956	0.983
$2d$	0.011	0.003	0.030	0.007
$3d$	0.006	0.001	0.019	0.006

TABLE II. The occupation numbers of the l–th natural orbits for ^{16}O and ^{40}Ca in CBF, with three correlation models and in the Green function (GF) approach.

	corr.	n_s	n_p	n_d	n_f
^{16}O	J	0.971	0.991	0.011	0.002
	f_4	0.977	0.988	0.015	0.004
	f_6	0.899	0.966	0.047	0.006
	GF	0.936	0.951	0.022	0.007
^{40}Ca	J	1.932	0.975	1.003	0.022
	f_4	1.907	0.964	1.005	0.022
	f_6	1.727	0.920	1.026	0.071

TABLE III. CBF spectroscopic factors for ^{16}O and ^{40}Ca, with Jastrow (J) and spin–isospin correlations, with (f_6) and without (f_4) tensor components.

	corr.	$1s$	$1p$	$1d$	$2s$
^{16}O	J	1.00	0.98		
	f_4	0.79	0.96		
	f_6	0.70	0.90		
^{40}Ca	J	0.98	0.99	0.97	0.98
	f_4	0.71	0.76	0.96	0.97
	f_6	0.55	0.58	0.87	0.86

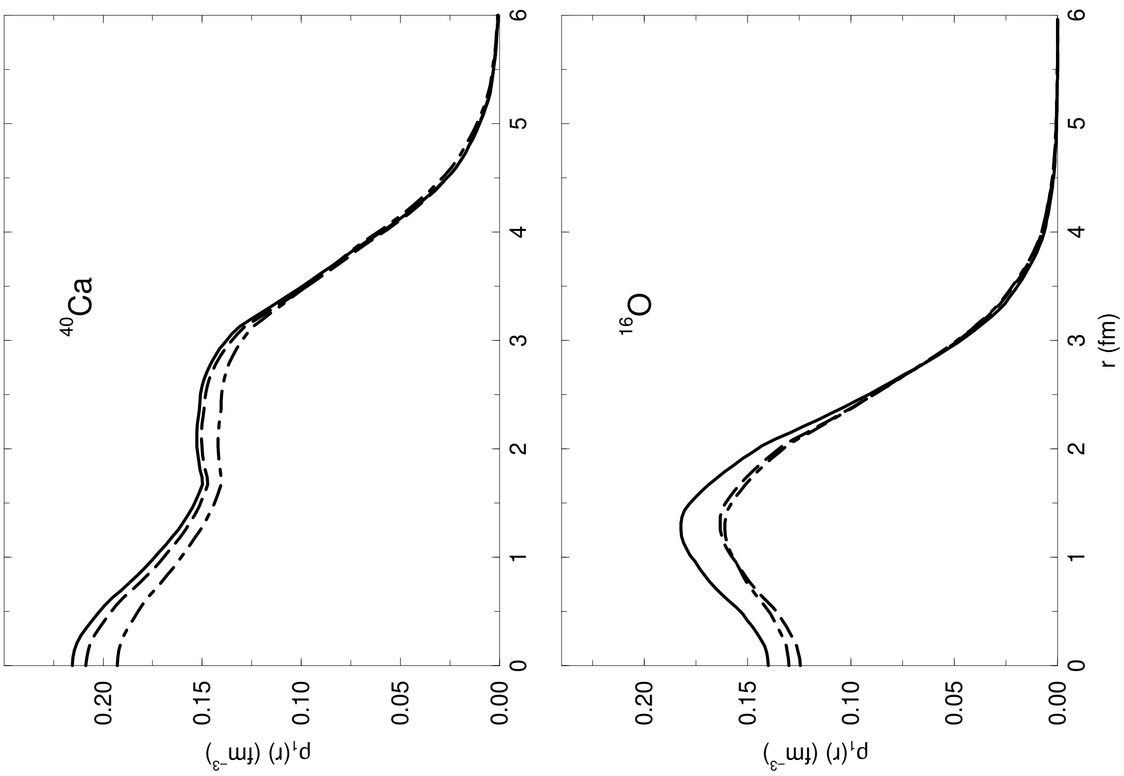

FIG. 1. Nuclear one body densities. The solid lines are the FHNC/SOC results with the f_6 correlation, the dot–dashed lines are the densities with the Jastrow correlation, the dashed lines are the IPM densities.

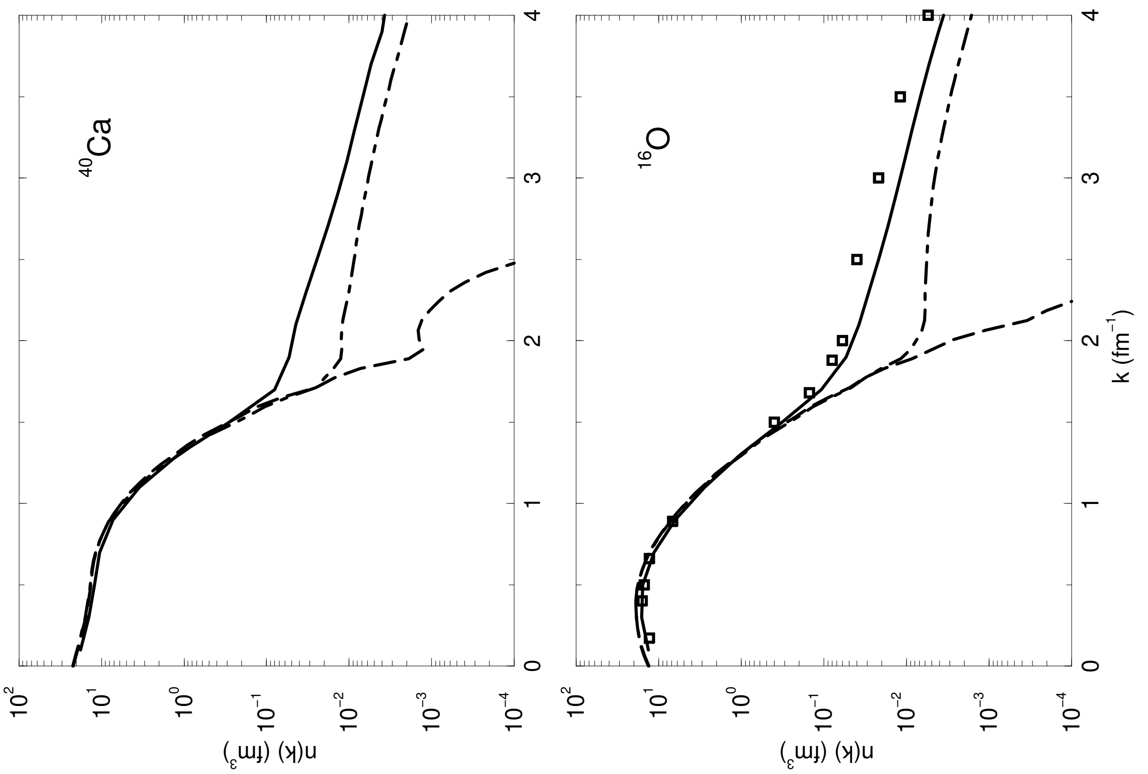

FIG. 2. FHNC/SOC momentum distributions in ^{16}O and ^{40}Ca. Solid lines: f_6 model; dot–dashed: Jastrow; dashed: IPM. The squares are the VMC results of Ref. [8].

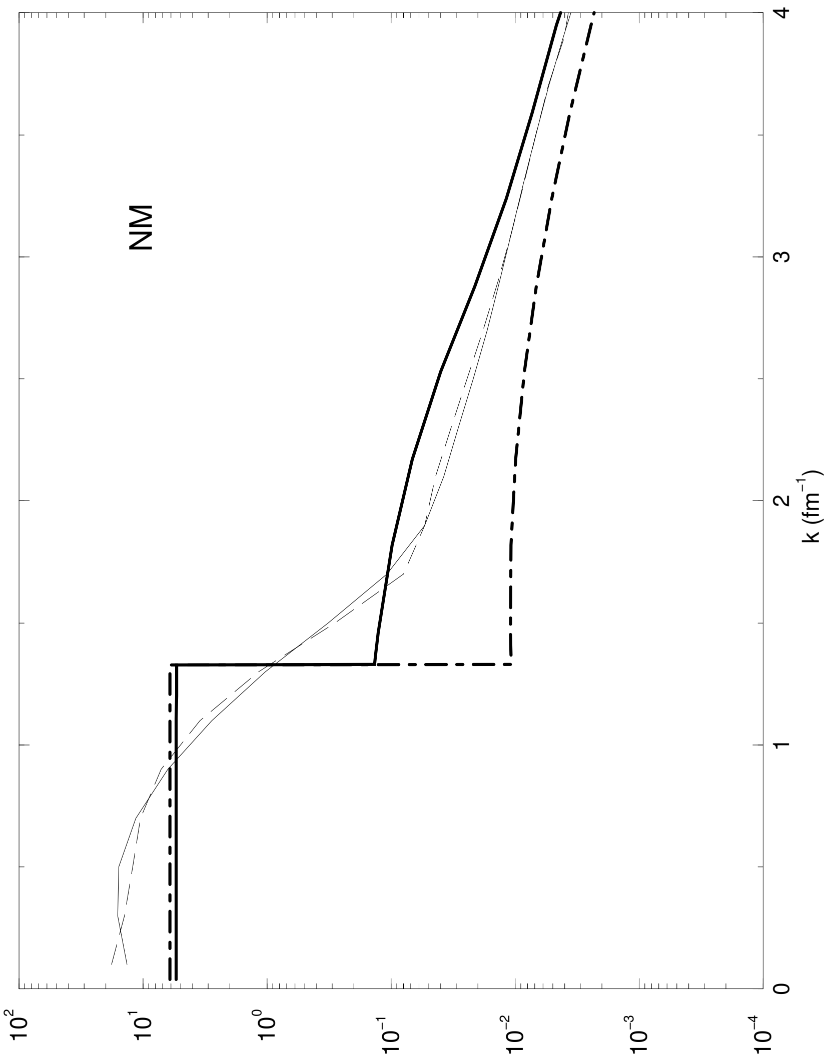

FIG. 3. FHNC/SOC momentum distributions in ^{16}O, ^{40}Ca and nuclear matter (NM). Solid line: NM f_6 model; dot–dashed: NM Jastrow model; thin solid line: ^{16}O f_6 model; thin dashed line: ^{40}Ca f_6 model.

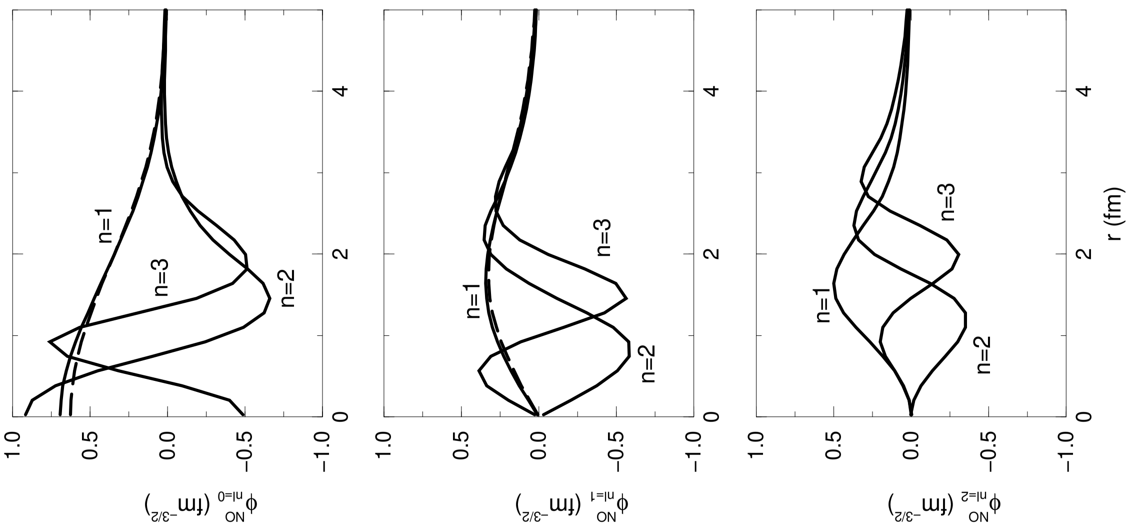

FIG. 4. ^{16}O natural orbits. Solid lines: f_6 model; dashed: IPM.

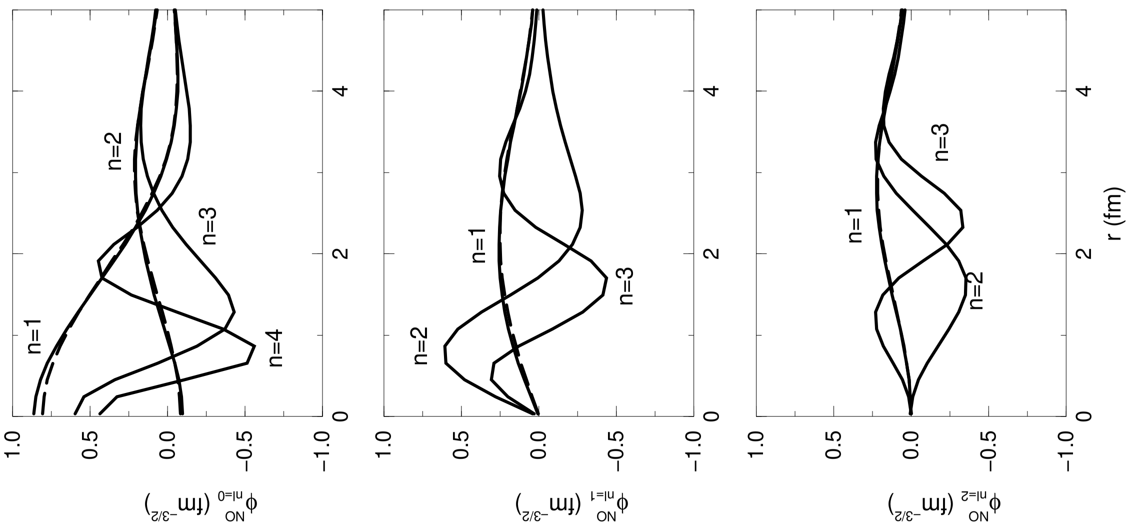

FIG. 5. ^{40}Ca natural orbits. Solid lines: f_6 model; dashed: IPM.

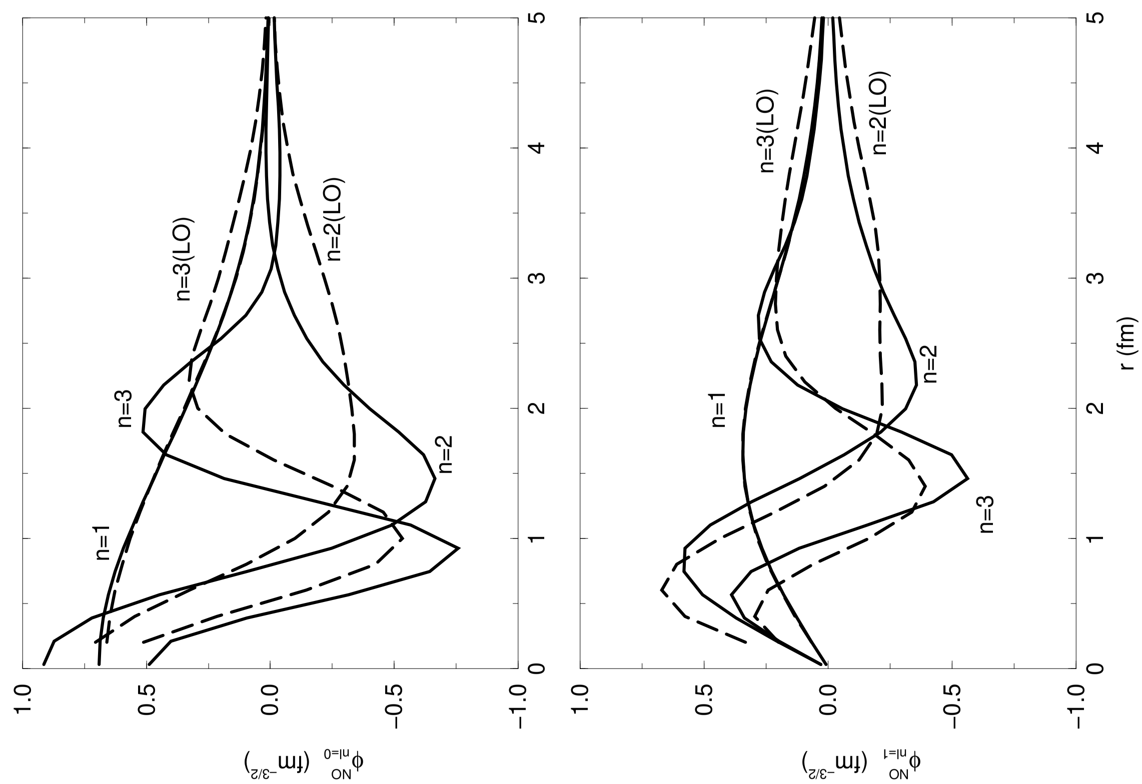

FIG. 6. ^{16}O l =0, 1 natural orbits in FHNC/SOC (solid lines) and LO approximation (dashed lines).

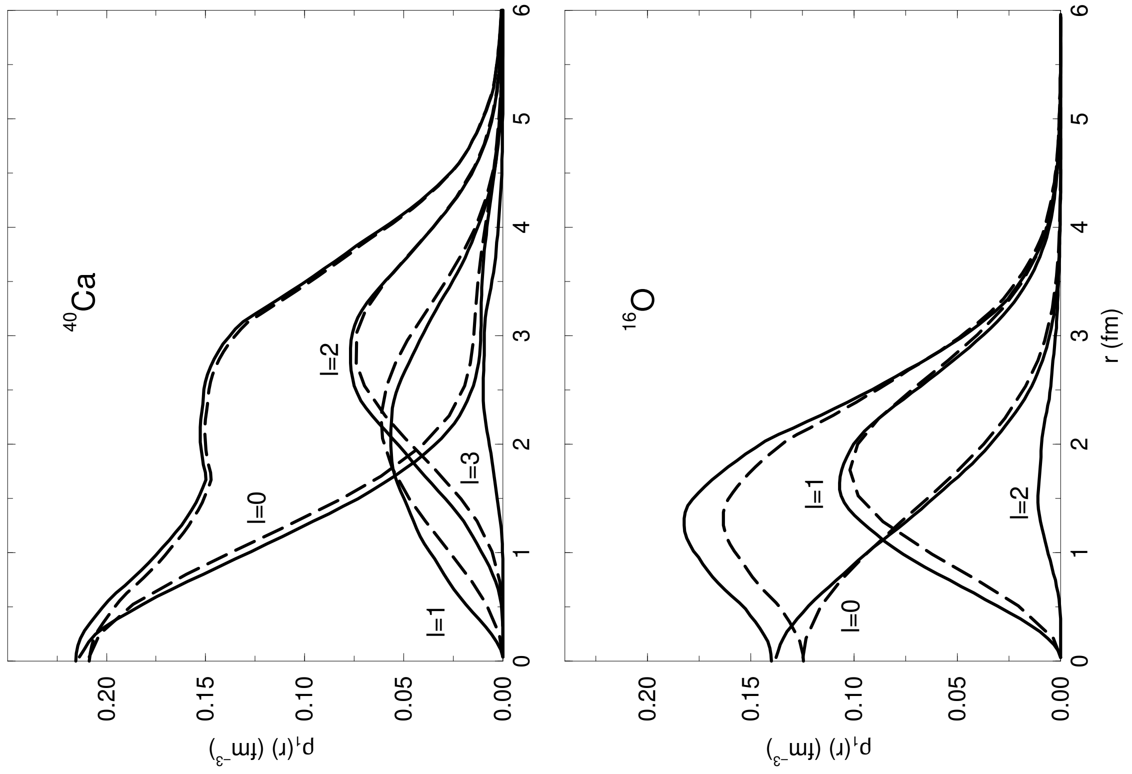

FIG. 7. Partial wave contributions to the one body densities in the natural orbits representation. The upper lines are the total densities. The remaining lines give $\nu \frac{2l+1}{4\pi} \rho_l(r, r)$. Solid lines: f_6 model; dashed: IPM.

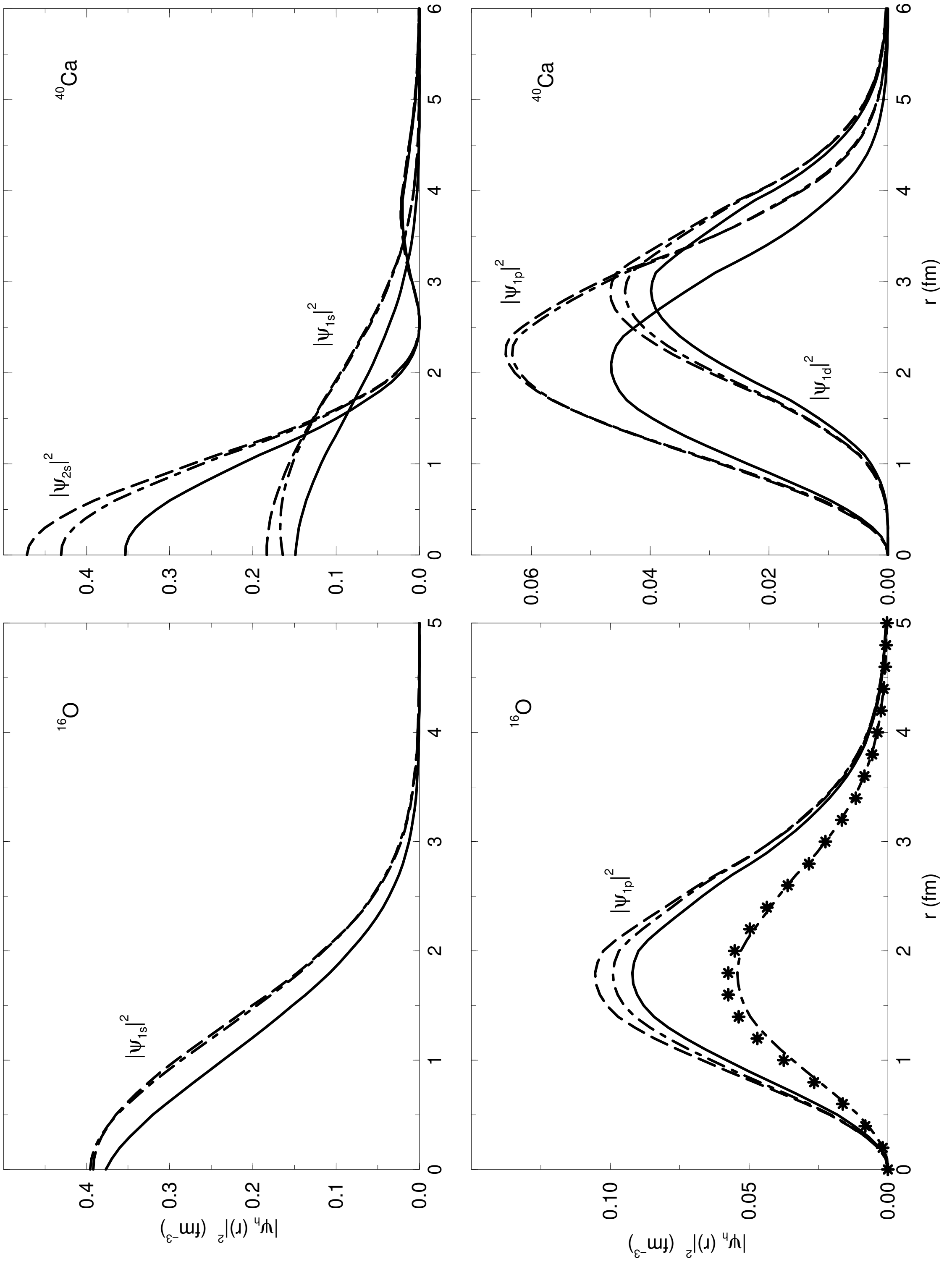

FIG. 8. Squared quasihole wave functions. Solid lines: f_6 model; dot–dashed: Jastrow; dashed: IPM. The $1p$ panel of ^{16}O shows also the empirical overlap (stars) and the f_6 one, rescaled as explained in the text (lower dot–dashed line)

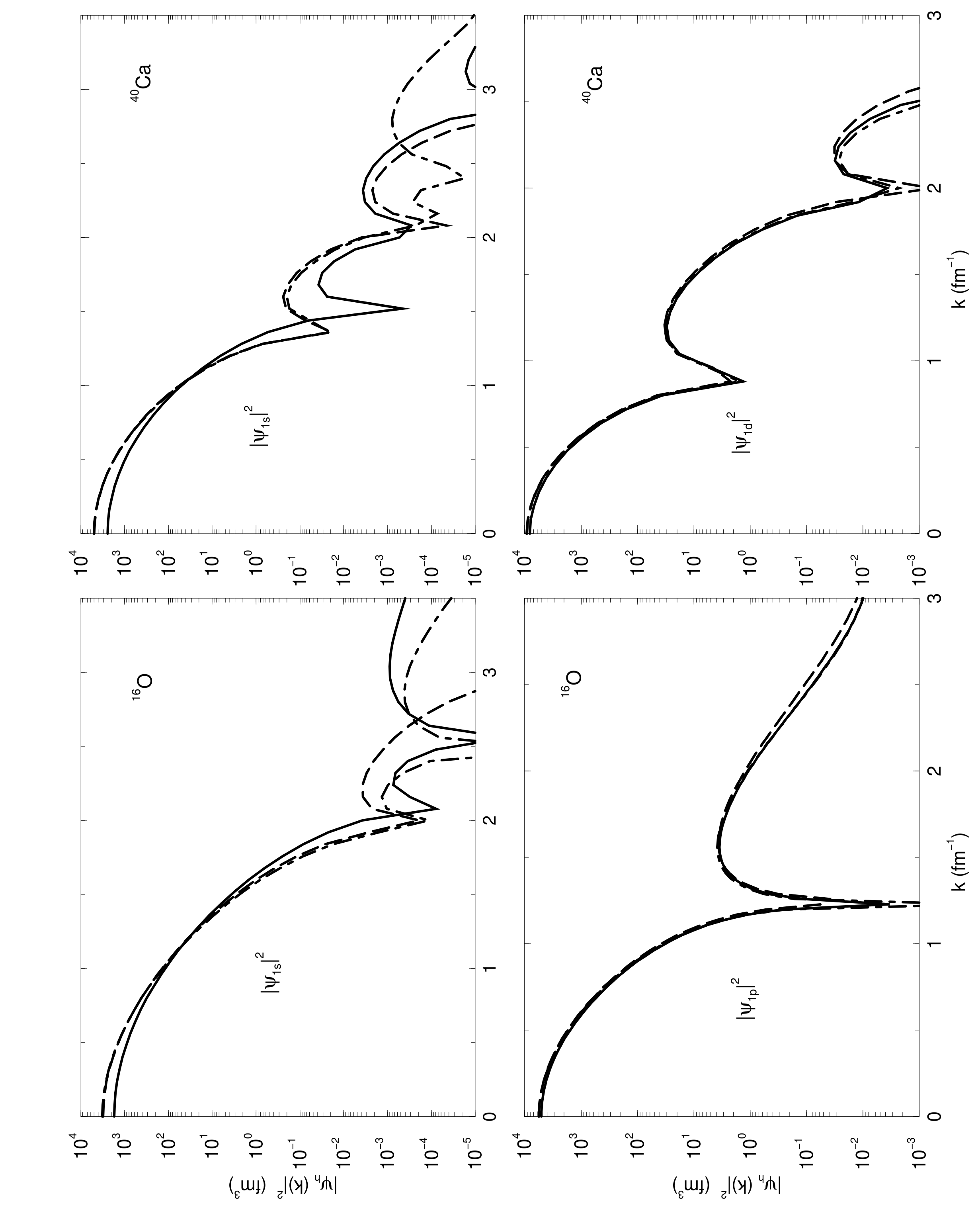

FIG. 9. Squared transform of the quasihole wave function for ^{16}O and ^{40}Ca. Solid lines: f_6 model; dot–dashed: Jastrow; dashed: IPM.